



Journal of Geophysical Research: Atmospheres

RESEARCH ARTICLE

10.1002/2016JD025882

Key Points:

- HO₂ uptake coefficients measured on synthetic amorphous olivine particles
- Exposed surface Fe atoms appear to catalyze HO₂ removal to form H₂O₂
- Uptake on meteoric smoke significantly impacts the HO₂ atmospheric abundance over the winter poles

Correspondence to:

J. M. C. Plane, j.m.c.plane@leeds.ac.uk

Citation:

James, A. D., D. R. Moon, W. Feng, P. S. J. Lakey, V. L. Frankland, D. E. Heard, and J. M. C. Plane (2017), The uptake of HO_2 on meteoric smoke analogues, *J. Geophys. Res. Atmos.*, 122, 554–565, doi:10.1002/2016JD025882.

Received 1 SEP 2016 Accepted 15 NOV 2016 Accepted article online 17 NOV 2016 Published online 13 JAN 2017

The uptake of HO₂ on meteoric smoke analogues

Alexander D. James¹, Daniel R. Moon¹, Wuhu Feng^{1,2}, Pascale S. J. Lakey^{1,3}, Victoria L. Frankland¹, Dwayne E. Heard^{1,2}, and John M. C. Plane¹

¹School of Chemistry, University of Leeds, Leeds, UK, ²National Centre for Atmospheric Science, University of Leeds, Leeds, UK, ³Max Planck Institute for Chemistry, Mainz, Germany

Abstract The kinetics of heterogeneous HO_2 uptake onto meteoric smoke particles (MSPs) has been studied in the laboratory using analogues of MSP aerosol entrained into a flow tube. The uptake coefficient, γ , was determined on synthetic amorphous olivine (MgFeSiO₄) to be $(6.9 \pm 1.2) \times 10^{-2}$ at a relative humidity (RH) of 10%. On forsterite (Mg₂SiO₄), $\gamma = (4.3 \pm 0.4) \times 10^{-3}$ at RH = 11.6% and $(7.3 \pm 0.4) \times 10^{-2}$ at RH = 9.9% on fayalite (Fe₂SiO₄). These results indicate that Fe plays a more important mechanistic role than Mg in the removal of HO₂ from the gas phase. Electronic structure calculations show that Fe atoms exposed at the particle surface provide a catalytic site where HO₂ is converted to H₂O₂ via an Eley-Rideal mechanism, but this does not occur on exposed surface Mg atoms. The impact of this heterogeneous process in the middle atmosphere was then investigated using a whole atmosphere chemistry-climate model which incorporates a microphysical treatment of MSPs. Using a global MSP production rate from meteoric ablation of 44 t/day, heterogeneous uptake (with $\gamma = 0.2$) on MSPs significantly alters the HO_x budget in the nighttime polar vortex. This impact is highly latitude dependent and thus could not be confirmed using currently available satellite measurements of HO₂, which are largely unavailable at latitudes greater than 70°.

1. Introduction

A significant discrepancy exists between observations and model predictions of HO_2 concentrations in the middle atmosphere, known as the " HO_x dilemma" [Millán et al., 2015]. Siskind et al. [2013] showed that increasing the rate coefficient for the reaction

$$H + O_2(+ M) \rightarrow HO_2$$
, where $M = N_2$ or O_2 (1)

554

by a factor of \sim 1.5 improved agreement to the observed OH profile but did not present a detailed comparison for HO₂. *Pickett et al.* [2008] found that for northern hemisphere summer, rate constants within the stated error of the Jet Propulsion Laboratory 2006 recommendation could explain the observed HO₂ but did not discuss other seasons or latitudes. In general, a kinetic description which underpredicts HO₂ density in the upper mesosphere results in overprediction in the lower mesosphere/stratosphere and vice versa [*Millán et al.*, 2015].

The modeling studies discussed above consider only gas-phase chemistry. In terms of heterogeneous chemistry, noctilucent clouds occur in the polar summer mesosphere above 80 km, causing perturbations to atomic O and HO_x around the ice clouds [*Murray and Plane*, 2005]. However, in the middle mesosphere below 80 km the only known source of potentially reactive surfaces are meteoric smoke particles (MSPs). These particles form by recondensation of the metallic vapors, which are released by meteoric ablation [*Hunten et al.*, 1980; *Plane et al.*, 2015] and are likely composed of Fe-Mg silicates [*Saunders and Plane*, 2006]. Recent studies have shown that uptake on MSPs may significantly affect the atmospheric abundance of species such as HNO₃ and H₂SO₄ in the stratosphere/lower mesosphere [*Frankland et al.*, 2015; *Saunders et al.*, 2012]. The heterogeneous recombination of O and H₂ on MSPs has also been suggested as a source of H₂O in the lower mesosphere [*Summers and Siskind*, 1999].

A study of the heterogeneous chemistry of HO_2 on MSPs is therefore timely. Here we report an experimental measurement of the uptake coefficient, γ , for HO_2 on a variety of MSP analogues, which were prepared using a sol-gel process that we have described previously [Frankland et al., 2015]. The uptake rate was measured by entraining these particles in a laminar gas flow and detecting HO_2 by conversion to OH and the Fluorescence Assay by Gas Expansion (FAGE) technique [Matthews et al., 2014].

The Fluorescence Assay by Gas Expansion (FAGE) technique is used to detect HO₂ radicals with very high sensitivity, building from extensive experience in measuring these radicals in the field [Stone et al., 2012].

©2016. American Geophysical Union. All Rights Reserved.



Briefly, gas is sampled at the end of the aerosol flow tube by a small circular pinhole (diameter 0.7 mm), at which point the gas expands supersonically into a low-pressure fluorescence cell, and the gas jet is crossed by a laser beam ~120 mm from the pinhole. The background pressure in the cell is held at ~1 torr, with the fast flow of gas maintained by a rotary pump/root blower combination, and close to the pinhole nitric oxide (NO; 99.5% black organic carbon) is added to convert HO₂ to OH radicals, which are detected by laser-induced fluorescence exciting at a wavelength of ~308 nm (from a high-pulse-repetition-frequency, neodymium: yttrium/aluminum/garnet-pumped dye laser) using the $Q_1(2)$ rotational transition of the $A^2\Sigma$ (v'=0) – $X^2\Pi_{3/2}$ (v''=0) vibronic band of OH. On-resonant fluorescence is collected via the same band, using a series of fast lenses and an interference filter centered at 308 nm, and in order to discriminate against the more intense, laser-scattered light, the fluorescence, whose lifetime is extended at the low pressure, is detected via delayed photon counting. The detector (PerkinElmer 993P) is gated off during the laser pulse to avoid saturation from the scattered light. The sensitivity of the HO₂ detection is calibrated using a known concentration of HO₂ generated from the photolysis of water vapor at 185 nm in presence of zero air [Whalley et al., 2011; George et al., 2013; Matthews et al., 2014] and is ~10⁶ molecules cm⁻³.

A version of the Whole Atmosphere Community Climate Model (WACCM) coupled with the Community Aerosol and Radiation Model for Atmospheres (CARMA), which includes a treatment of MSP microphysics [Bardeen et al., 2008], was then used in order to determine if MSPs can have an impact on the HO_x budget. Because of uncertainties in the uptake coefficients this study does not attempt to quantify any such impact. Rather, the modeling presented here is intended to give the reader an idea of when and where such an impact might occur.

2. Experimental Method

MSP analogues in the form of amorphous compounds with olivine compositions $Mg_xFe_{2-x}SiO_4$ (where $0 \le x \le 2$) were produced by mixing stoichiometric quantities (relative to 0.1 molar product) of aqueous solutions of magnesium chloride (Aldrich), ferrous (II) ammonium sulfate (Sigma-Aldrich), and sodium orthosilicate (Alfa Aesar) at room temperature for 7 days [Frankland et al., 2015]. Metal-salt by-products were removed from products by repeated dialysis using a soxhlet apparatus with the particles held in water-permeable tubing (Snakeskin 7000 molecular weight cutoff). This method was used to produce materials with x = 0, 1, and 2. Although the products are amorphous, they will hereafter be referred to, respectively, as fayalite, olivine, and forsterite for simplicity.

The experimental procedure for measuring the HO_2 uptake coefficients has been described in detail elsewhere [George et al., 2013; Matthews et al., 2014]. An experimental diagram is shown in Figure 1.

Details of the gas flow control system are given in *Matthews et al.* [2014], which described uptake experiments onto Arizona Test Dust aerosols. The carrier gas used for these experiments was compressed nitrogen, which first passed through a gas purification system consisting of particle filters, a dryer, and a carbon filter. The HO_2 flow, the humidified flow, and the NO flow were controlled using five mass flow controllers (Brooks, model 5850S and MKS, model 1179A). The required relative humidity (RH) was obtained by mixing together and altering the ratio of a dry flow and a flow which had been passed through a water bubbler (Milli-Q, 18 M Ω cm). This humidified flow, which was mixed with the aerosol flow in the conditioning flow tube, was ~3 liters per minute (Lpm) throughout each individual experiment. The aerosol flow was monitored and maintained at 1.0 ± 0.1 Lpm, and the HO_2 flow from the injector (which is moved to provide varied contact times in random order) was measured as 1.3 ± 0.05 Lpm. The total flow passing through the flow tube (with 5.9 cm diameter), including the aerosol, dilution, and HO_2 flows, was $\sim 5.3 \pm 1$ Lpm (variations are due to the mixing of dry and humid flows). The FAGE instrument sampled ~ 4.2 Lpm, and the condensation particle counter (CPC; TSI 3775) sampled 0.3 Lpm with the remainder of the flow (~ 0.8 Lpm) exiting via an exhaust line. The pressure and temperature in the aerosol flow tube were maintained at atmospheric pressure and room temperature ($\sim 20-22^{\circ}C$).

MSP aerosols were entrained in the carrier gas using either a magnetic stirrer (shown in Figure 1) or acoustic dust disperser and passed through an impactor (TSI 1034900, nozzle diameter 0.71 mm, D_{50} = 1286 nm), which was used to stabilize the flow rate from the dust disperser. The concentration of aerosols entering the flow tube was controlled using a high-efficiency particulate air filter and a bypass. The proportion of the flow passing through the bypass compared to the filter was controlled using a needle valve (not shown in Figure 1). The

556



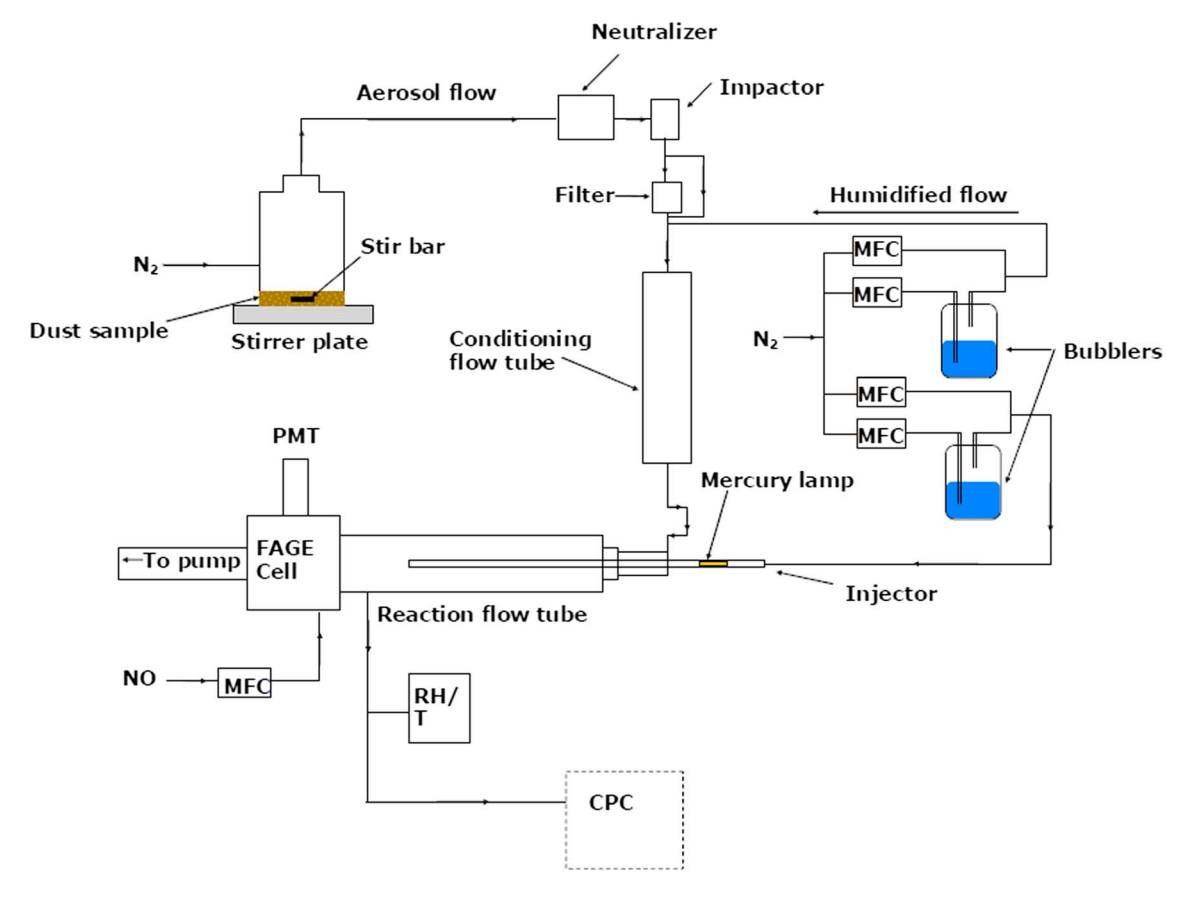


Figure 1. Schematic diagram of the experimental system. Abbreviated components: condensation particle counter (CPC), mass flow controller (MFC), and photomultiplier tube (PMT).

aerosol number concentration was monitored using a CPC. Measurements were also made either immediately before or after each uptake experiment, under the same experimental conditions, using a Scanning Mobility Particle Sizer (SMPS; TSI 3080) in order to measure the entire lognormal size distribution. Checks determined that the average radius did not change over time or when sampling from before or after the flow tube. The size distribution was independent of whether HO₂ was flowing from the injector or not.

HO₂ was formed by passing water vapor in front of a mercury pen lamp to form OH and H; HO₂ is then produced when the latter reacts with trace O_2 impurity in the N_2 carrier gas. This produces an initial HO_2 concentration in the second flow tube of 1.6×10^9 molecules cm⁻³. Variability in the HO₂ signal due to lamp output and supplied humidity (controlled by flow controllers) is very small. The absolute concentration downstream is known following calibration of the sensitivity of the fluorescence cell [George et al., 2013]. The injector was used to vary the contact time of the HO₂ with the aerosol to determine the uptake kinetics. Experiments were performed on all three MSP analogue materials.

3. Results and Discussion

3.1. Measured Size Distributions

A typical set of 10 measured size distributions is shown for fayalite at 9.9% RH in Figure 2. The mean, which is used to calculate the experimental surface area, is shown in black. This shows that, while there is some variability in the output of the aerosolizer, a lognormal distribution is measured and can be well characterized (in this case the distribution had a mean of 368 nm and a standard deviation of 0.680). This gives a measurement of the mean surface area of each MSP $(4.25 \times 10^{-9} \text{ cm}^2 \text{ in this example})$. CPC measurements of the number concentration are used during experiments to calculate the total available surface area.

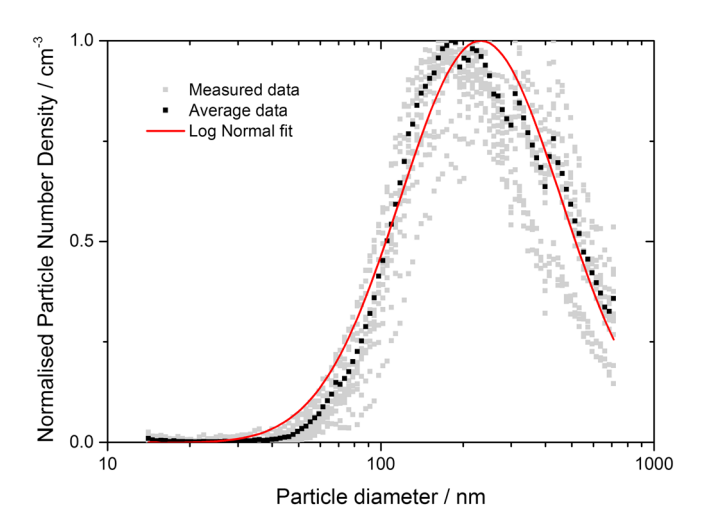


Figure 2. Measured size distribution of fayalite at 9.9% RH, normalized to the peak of a lognormal fit to the distribution. Ten individual measurements are shown in grey with the mean in black and a lognormal fit (mean and standard deviation of 368 nm and 0.680, respectively) to the size distribution in red.

The spherical assumption used here for the particles neglects any surface roughness and may lead to an underestimation of the surface area available for HO₂ to interact with. This would result in an overestimation of the uptake coefficient [Frankland et al., 2015].

3.2. Measurements of the Uptake Coefficient

A clear uptake of HO₂ to the MSP analogues was observed in all experiments. Figure 3a illustrates the relationship between the fayalite aerosol number concentration and HO₂ signal in a typical experiment, where the RH was 9.9% and residence time of 20.6 s. Raw HO₂ signal is shown. Before further analysis the data were corrected for the output

power of the laser. The reference cell signal would also enable any drifts in laser power or wavelength to be monitored and is used to center the laser wavelength on the OH transition. If the reference cell changes significantly (but not the laser power), then the data are not used so the laser power is considered a good reference for normalization. Since uptake is a first-order process, the HO_2 concentration $[HO_2]_t$ is then related kinetically to the available aerosol surface and the initial concentration $[HO_2]_0$ by

$$-\ln \frac{[HO_2]_t}{[HO_2]_0} = 0.25 \ \gamma_{obs} w A_d N_d t + k_W t$$
 (2)

where $\gamma_{\rm obs}$ is the observed uptake coefficient, w is the molecular mean speed (cm s⁻¹), N_d is the number density of aerosol (cm⁻³), A_d is the surface area of the mean aerosol particle (cm²), t is the contact time (s) during which HO₂ can adsorb onto the particles, and k_w is the rate coefficient for loss (s⁻¹) of HO₂ on the flow tube walls and by self-recombination in the gas phase to form H₂O₂. This is determined by measuring uptake without the aerosol flow for several injector positions at the beginning and end of each experiment (under the same RH conditions). It should be noted that at HO₂ concentration of ~10⁹ molecules cm⁻³ the loss via the gas phase reaction is very small (e-folding lifetime >100 s). At the pressure of 1 bar used in these experiments, diffusional transport of HO₂ to the particle surface is not in the free molecular regime, so $\gamma_{\rm obs}$ was then corrected for slip flow [Matthews et al., 2014]:

$$\gamma = \frac{\gamma_{\text{obs}}}{1 - \gamma_{\text{obs}}\lambda(r_{\text{s}})} \tag{3}$$

where $\lambda(r_s)$, the mean free path for a particle of radius r_s , is given by

$$\lambda(r_s) = \frac{0.75 + 0.28Kn}{Kn(1 + Kn)} \tag{4}$$

where Kn, the Knudsen number, is given by

$$Kn = \frac{3D_g}{Wr_s} \tag{5}$$

and D_g is the diffusion constant for HO₂, taken to be 0.25 cm² s⁻¹ at 1 bar [Mozurkewich et al., 1987]. This results in a range of Kn from 1.26 for the smallest to ~0.3 for the largest particles. The contact time t was determined for the experimental flow conditions (Reynolds number = 136) by applying the Brown correction to the plug flow time determined from the mass flow rates and pressure [Brown, 1978]. Figure 3b shows that $ln[HO_2]_t$ was linearly anticorrelated with N_{dt} in accordance with equation (2), so the slope is equal to 0.25 $\gamma_{\text{obs}} w A_d t$ ((6.3 \pm 1.4) \times 10⁻⁶ in this case). The slope was then measured over a range of contact times

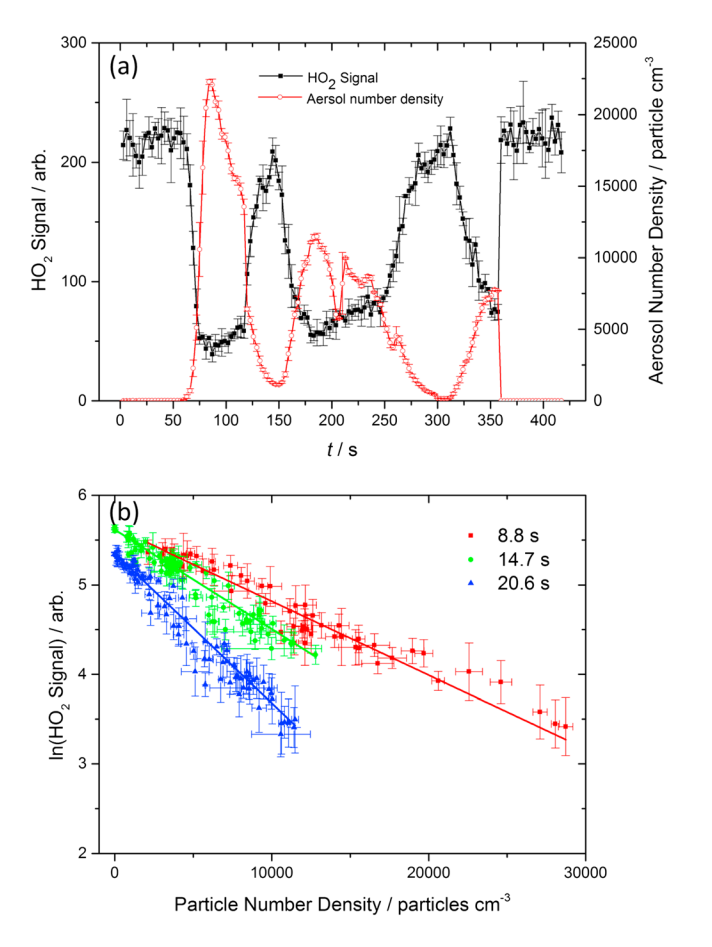


Figure 3. (a) Example plot showing the anticorrelation of HO_2 signal to number concentration of fayalite MSP analogue particles (at 9.9% RH with a residence time of 20.6 s). (b) Example plot showing the HO_2 signal variation with fayalite aerosol number concentration, also at 9.9% RH for three fixed contact times as shown in the legend. Full experimental conditions are given in the text. Means and standard deviations of three condensation particle counter and FAGE measurements are shown (as points and error bars, respectively).

and found to vary linearly as shown in Figure 4a (for fayalite at RH of 9.9%, $R^2 = 0.945$). The mean aerosol surface area determined from a lognormal fit to the SMPS data and the gradient of the line in Figure 4a was used to determine γ .

Matthews et al. [2014] suggested that a positive intercept on a plot such as Figure 4a can be indicative of some experiments occurring at contact times too short for HO2 to reach equilibrium with the surface. By plotting a line from the origin to each point in Figure 4a, the change in uptake coefficient over time can be quantified. This is shown in Figure 4b. Some surface sites in these experiments appear to be deactivated as the HO2 comes to equilibrium with the MSP analogues. The probability of uptake is less at equilibrium (when some sites are occupied) than for surfaces which have had contact times too short to reach equilibrium. Note that the uptake coefficient at long times approaches that calculated from the fit to the whole data set. These values should be taken as the true measurement of uptake, since they correspond to HO₂ in equilibrium with the surface. Any change in the system as a result of the experimental process, e.g., deposition of analo-

gue particles in the flow tube, could also lead to changes in the intercept of plots such as Figure 4a, but since the measurements at different contact times are performed in random order this could not explain the observed larger uptake coefficients for points at shorter contact times.

Surface coverage of HO_2 can be further investigated by estimating the mean distance between HO_2 molecules on the surface at the longest contact times, assuming that all HO_2 which are taken up remain on the surface. This is done by integrating the loss of HO_2 with respect to time to determine the total adsorbed on dust of known surface area and assuming that the HO_2 molecules are dispersed isentropically over the surface. The smallest distance estimated here was 10 Å, implying that a significant proportion of the surface sites might have become saturated. However, the linearity of plots such as those shown in Figure 4a implies that there was no deviation from constant first-order uptake kinetics. This suggests that HO_2 is converted to other products and many of the available surface sites are reactivated. This is discussed further in the light of electronic structure calculations below.

Matthews et al. [2014] also found that the uptake coefficient decreased by a factor of 2 with a fourfold increase in the initial concentration of HO_2 . Since the mechanism in both cases is likely driven by Fe active sites [Broadley et al., 2012], we would expect a similar trend here. Equivalent experiments, which are technically challenging and cannot cover a large range of $[HO_2]_0$, were therefore not performed in this study. The γ values measured in this study are summarized in Table 1. The larger γ values measured on olivine and

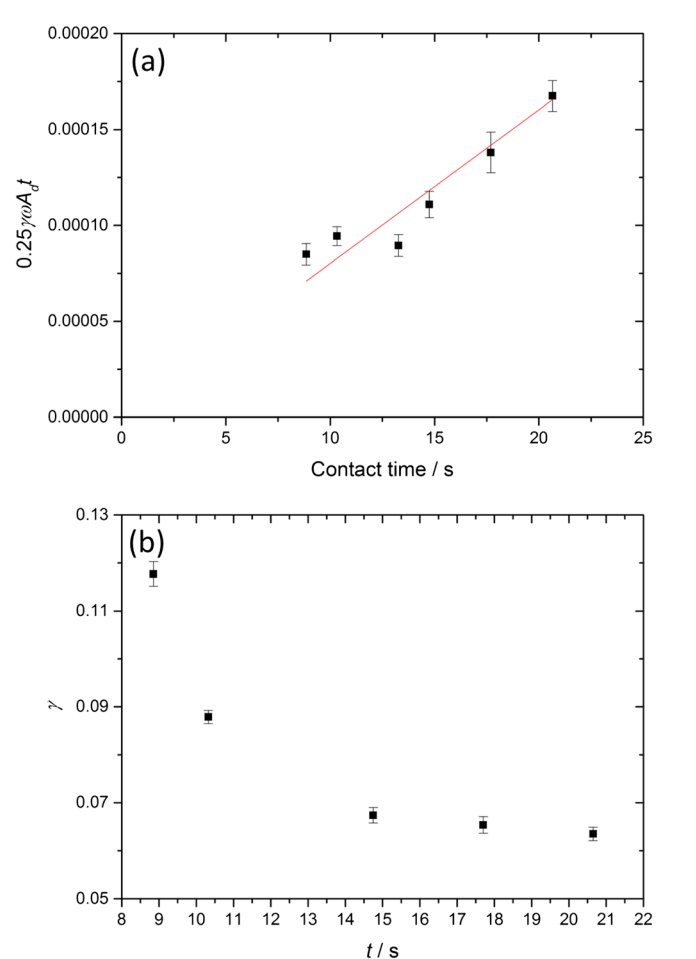


Figure 4. (a) Plot of the dimensionless quantity 0.25 $\gamma_{\rm obs}$ wA_dt as a function of reaction time for uptake of HO₂ onto fayalite at a RH = 9.9%. The linear least squares fit to these points yields 0.25 $\gamma_{\rm obs}$ wA_d as the gradient, $(6.3\pm1.4)\times10^{-6}$ in this case, from which $\gamma_{\rm obs}=(7.3\pm0.4)\times10^{-2}$ was obtained. The intercept of the fit at t=0 ((2.3 $\pm1.8)\times10^{-5}$) suggests a higher gradient and hence a higher uptake coefficient occurring in the first few seconds of contact between the HO₂ and fayalite aerosols. The error bars represent 2 standard deviations in the individual exponential fits; examples of which are given in Figure 3b. (b) Plot of $\gamma_{\rm obs}$ determined from a straight line from the origin to each point in Figure 4a, demonstrating that over time $\gamma_{\rm obs}$ decreases toward the value obtained from the straight line fit shown in Figure 4a.

fayalite suggest that HO_2 is taken up more readily by Fe compared with Mg active sites on the MSP analogue surface.

A number of previous studies have concluded that HO2 uptake could be driven by the presence of transition metal ions (TMIs) at the particle surface or in the bulk of a liquid particle [e.g., Lakey et al., 2015]. Mao et al. [2013] demonstrated that where Fe and Cu ions are both present in a liquid droplet redox chemistry can lead to the production of H₂O rather than H₂O₂. These mechanisms are not likely to be important here, however, since for TMIs to be available in a liquid droplet would require both RH approaching 100% and a soluble solid. Since by-products of the synthesis process are removed from the MSP analogues by repeated dialysis in near boiling point water, it is unlikely that any soluble material remains.

3.3. Electronic Structure Calculations

In order to investigate the mechanism for HO_2 uptake on the MSP analogue surfaces, we employed electronic structure calculations using the Gaussian 09 suite of programs [Frisch et al., 2009]. The hybrid density functional/Hartree-Fock B3LYP method was employed together with the 6–311+G(2d,p) triple zeta basis set, which is a reasonably large, flexible basis set with both polarization and diffuse functions added to the atoms. We have used

this level of theory previously for calculations on Fe- and Mg-containing oxides, hydroxides, and silicates [Rapp et al., 2012; Saunders and Plane, 2011]. The expected uncertainty in the calculated reaction enthalpies is $\pm 20 \,\mathrm{kJ} \,\mathrm{mol}^{-1}$ at this level of theory.

Since we are interested in the reactivity of HO_2 with exposed surface sites, here we consider the binding of HO_2 to either the Fe or Mg end of an FeMgSiO₄ unit. While this is clearly an approximation of the surface, it yields useful insights into the likely mechanisms that occur and is useful for interpreting the experimental observations. For

Table 1. Values of γ Measured in This Study			
MSP Analogue	RH/%	Measured γ	R ² (see Figure 4a)
Forsterite Olivine Fayalite	11.6 10.0 9.9	$(4.3 \pm 0.4) \times 10^{-3}$ $(6.9 \pm 1.2) \times 10^{-2}$ $(7.3 \pm 0.4) \times 10^{-2}$	0.953 0.985 0.945

each molecule the geometry was first optimized, and then vibrational frequencies were calculated to determine the zero-point energy correction. The most stable form of FeMgSiO₄ has quintet spin multiplicity [Saunders and Plane, 2011] because of

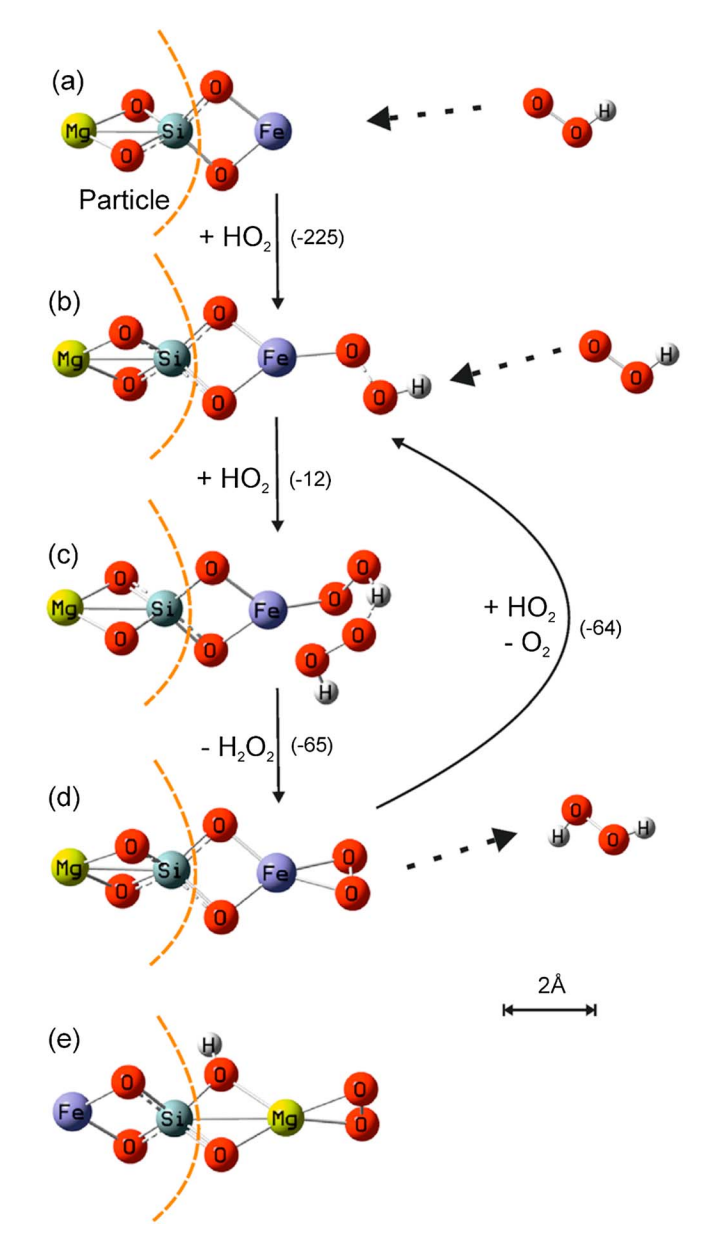


Figure 5. Electronic structure calculations at the B3LYP/6–311 + g(2d,p) level of theory with enthalpies in kJ mol $^{-1}$ in brackets: (a) HO $_2$ uptake on an exposed Fe atom on the olivine surface leads to a (b) chemisorbed adduct; (c) a second HO $_2$ can now abstract the adsorbed H atom via transition state to form, (d) where O $_2$ is bound to the Fe atom, which can then be displaced by a further HO $_2$ to yield (Figure 5b). (e) When HO $_2$ adds to an exposed Mg atom, chemisorption leads to the very stable structure.

the presence of the Fe atom. We therefore considered all possible spin multiplicities of the species involved in HO_2 uptake and subsequent reaction. The results for the most stable spin states are reported here (though in fact the different states of the relevant molecules are near-degenerate).

These calculations indicate that an exposed surface Fe atom is able to catalyze the destruction of HO₂ via the overall reaction

$$HO_2 + HO_2 \rightarrow H_2O_2 + O_2$$
 (6)

Figure 5 illustrates the catalytic mechanism. An HO₂ first chemisorbs to the Fe atom with a substantial binding energy of 225 kJ mol⁻¹ (Figures 5a and 5b). A second HO₂ can then abstract the adsorbed H atom, in a reaction that is quite exothermic $(\Delta H^0(0 \text{ K}) = -77 \text{ kJ mol}^{-1}).$ Note that the differing role of the two HO₂ radicals effectively makes the reaction first order, reconciling this mechanism with the kinetic plots shown above. This reaction occurs via a submerged transition state (Figure 5c) to yield H_2O_2 and an O_2 molecule bound to the Fe atom (Figure 5d). Finally, a third HO₂ can displace the bound O₂ exothermically $(\Delta H^{0}(0 \text{ K}) = -64 \text{ kJ mol}^{-1})$ to yield the structure in Figure 5b, hence starting the Eley-Rideal cycle over again.

In contrast, when HO_2 adsorbs onto an exposed Mg, the H atom migrates onto an O of the silicate group and the remaining O_2 is strongly bound to the Mg (Figure 5e). This process is even more exothermic than adsorption to the Fe, with $\Delta H^0(0~{\rm K}) = -342~{\rm kJ~mol}^{-1}$. However, the H atom cannot be abstracted via

a gas-phase HO_2 , because this is highly endothermic ($\Delta H^0(0 \text{ K}) = 106 \text{ kJ mol}^{-1}$), and the O_2 is too strongly bound to the Mg atom to be displaced. Thus, the adsorption effectively deactivates the Mg site.

These calculations therefore provide an explanation for two experimental observations: the much larger value of γ for fayalite compared with forsterite and the fact that the uptake rate on olivine and fayalite reach a steady state at large contact times.

3.4. Atmospheric Modeling

In order to explore the impact of HO_2 uptake on MSPs, we have used WACCM (extending vertically from the surface to 140 km) coupled with the CARMA aerosol microphysics model [Marsh et al., 2013]. This combination



has previously been used by Bardeen et al. [2008] to treat MSPs in the atmosphere and by Frankland et al. [2015] to examine the effect of uptake to MSPs on the HNO₃ budget. A cosmic dust input rate into the atmosphere of $44 \, \mathrm{t} \, \mathrm{day}^{-1}$ is used, and this all assumed to ablate and subsequently form MSPs. Model simulations for the years 2004-2010 were carried out with specified dynamics using a meteorological data set from Goddard Earth Observing System model version 5 below 50 km. Dynamics were specified as in Feng et al. [2013], so that 1% of the meteorological conditions (temperature, winds, surface pressure, specific humidity, surface wind stress, latent, sensible heat flux, etc.) was combined with the WACCM fields below 50 km at every model dynamic time step. This nudging factor then reduced linearly from 1 to 0% between 50 and 60 km. Above 60 km there is no nudging to the reanalysis fields, and the model in this region is free-running. Two WACCM-CARMA simulations were run: a control experiment with no uptake of HO_2 to MSPs and a second experiment where removal was added using $\gamma = 0.2$. Comparison of the two runs then allows assessment of the importance of this process.

This study aims to demonstrate an impact of MSP on the atmospheric availability of HO₂ in terms of when and where an impact would be observable. Quantification of such an impact is not an aim since uncertainties in the uptake coefficient are both too large and too complex [Frankland et al., 2015]. The available surface area of MSP is also uncertain, both in terms of the total mass influx and the fractal agglomerate nature of the atmospheric particles [Plane, 2012; Saunders et al., 2007].

An uptake coefficient (see equation (7)) for the atmospheric modeling was chosen as follows. Recent measurements have shown that HO₂ uptake tends to be more rapid for higher RH [see Lakey et al., 2015, Figure 3; Matthews et al., 2014, Figure 6]. This is either due to dissolution of TMI (although note that as droplet size increases, the concentration of TMI decreases so that the uptake would begin to reduce again in large droplets) or a HO₂.H₂O complex may form on the surface and react more rapidly than HO₂ radicals in a similar mechanism to that proposed for the gas phase [Stone and Rowley, 2005]. Although the middle atmosphere is relatively dry, significant RH can be reached at low temperatures. This occurs both in the summer mesosphere, where RH exceeds 100% and polar mesospheric ice clouds can form [Murray and Jensen, 2010], and in the winter stratosphere, where RH can reach 20%. This is demonstrated below in Figure 6b, where the RH from the WACCM control run is shown zonally averaged at 80°S as a function of pressure and time. For the most part, however, the middle atmosphere is significantly dryer than it is possible to measure using the current apparatus since H₂O is required to produce HO₂. Nevertheless, as the ambient conditions move toward low RH a kinetic steady state will be reached, where a mechanism not involving H₂O will dominate. This will cause the uptake coefficient to stabilize, as seen for example in measurements on humic acid [Lakey et al., 2015, Figure 3]. The uptake coefficient of ~0.07 measured here on olivine and fayalite likely holds for lower RH at room temperature. At colder atmospheric temperatures this is likely to increase [Mao et al., 2010]. Measuring γ at other atmospheric temperatures was not possible with the apparatus used in this study; however, it has been noted that γ usually increases with decreasing temperature [Hayward et al., 1967].

Parameter γ = 0.2 has therefore been used in the WACCM-CARMA model. This is a physically reasonable value (γ as high as 0.8 have been measured in the past for HO₂ uptake on aqueous aerosol [*Thornton and Abbatt*, 2005]). Such high values have previously been measured on solid aerosols only when significant Cu is present; however, Fe and other transition metals are also known to take up HO₂ efficiently [*Mao et al.*, 2010].

There is considerable uncertainty in the total amount of cosmic dust entering the atmosphere each day [Rapp et al., 2012], and the fraction that ablates is a function of the dust size and velocity distributions. Hence, it is possible that the value of the ablated mass input is higher by up to a factor of 3 [Carrillo-Sánchez et al., 2015], which would result in a larger modeled impact of MSP on the HO_2 abundance. Besides the uncertainty in the total MSP mass Saunders et al. [2007] showed that MSPs likely consist of fractal chain aggregates, which would imply that the surface area they present for reaction would be significantly higher than the spherical approximation used in the current modeling scheme. MSPs were input to WACCM-CARMA simulations as 0.2 nm radius primary particles (approximately molecular dimensions) injected over a range of altitudes between 75 and 110 km, with the peak injection rate at 83 km. Particles were then allowed to agglomerate collisionally and the surface area calculated in each model time step.

The rate of uptake to an atmospheric aerosol is defined by

$$\frac{d[HO_2]}{dt} = -0.25 \ w\gamma A_d[HO_2] \tag{7}$$

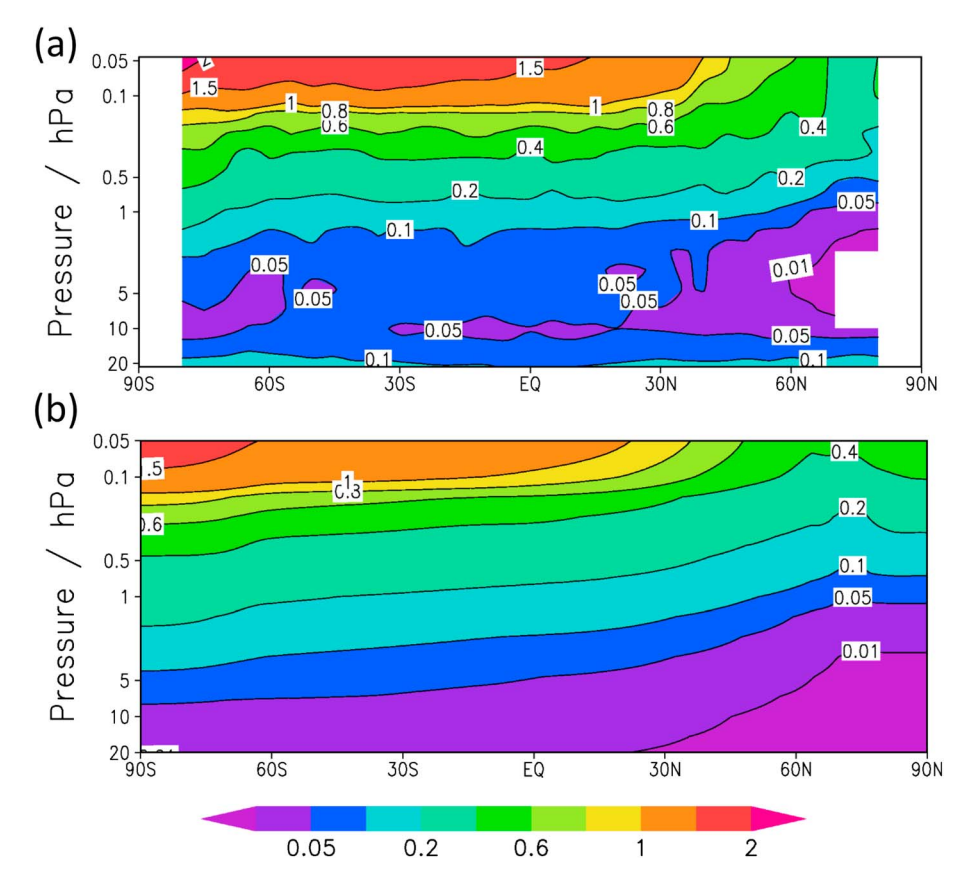


Figure 6. (a) Zonal average HO₂ mixing ratio (ppbv) as measured by the Microwave Limb Sounder (MLS) for January 2005. (b) Zonal average HO₂ mixing ratio (ppbv) as predicted by WACCM-CARMA simulations using specified dynamics for January 2005, from a control simulation with no heterogeneous uptake of HO₂. The color bar applies to both plots but should be interpreted with caution since a nonlinear color scaling has been used to display the full range of the data.

where A_d (cm² cm⁻³) is the volumetric surface area of aerosol available in the atmosphere. Note that equation (2) is the solution to an equation of a similar form to equation (7) but differs in that the former must account for losses, both to the flow tube walls and through gas phase self-recombination, and considers a mean aerosol particle. In addition, at the low pressures (uptake in the model occurs at pressures below 5 hPa; see below) present in the middle atmosphere the effect of diffusion can be neglected.

To assess the validity of this modeling approach, WACCM-CARMA output for the run with no $\rm HO_2$ uptake to MSPs was then compared to atmospheric observations from the Microwave Limb Sounder (MLS data version 4.2x), a radiometer aboard the Aura satellite [Livesey et al., 2013; Pickett et al., 2008; Waters et al., 2006]. All WACCM-CARMA data have been sampled at the averaging kernels used for the MLS data. This reduced the model altitude resolution in the stratosphere but allows a like with like comparison. A comparison for January 2005 is shown in Figure 6. The altitude range of both data sets has been displayed only to the recommended scientifically valid range of the MLS data (22–0.046 hPa, ~30–60 km). This is also a reasonable restriction to the WACCM-CARMA data as above this altitude nudging to the specified dynamics is not applied, while below this MSPs will be entrained in liquid sulfuric acid droplets and unable to take up $\rm HO_2$. The comparison in general is satisfactory: the $\rm HO_2$ mixing ratio increases with altitude and is fairly uniform across midlatitudes. The reduction and increase in the winter and summer polar regions, respectively, are well reproduced by the model.

WACCM-CARMA does appear to underpredict the mixing ratio at the higher altitudes (around 0.05 hPa) and overpredict at lower altitudes (around 5 hPa). A similar underestimation at high altitude was observed by *Millán et al.* [2015], who made an extensive comparison of WACCM to an off-line retrieval of MLS HO₂ mixing ratio, which was able to cover a larger range of altitudes than the data used here. The authors in that study speculated that either our understanding of mesospheric chemistry is incomplete or that parameterizations

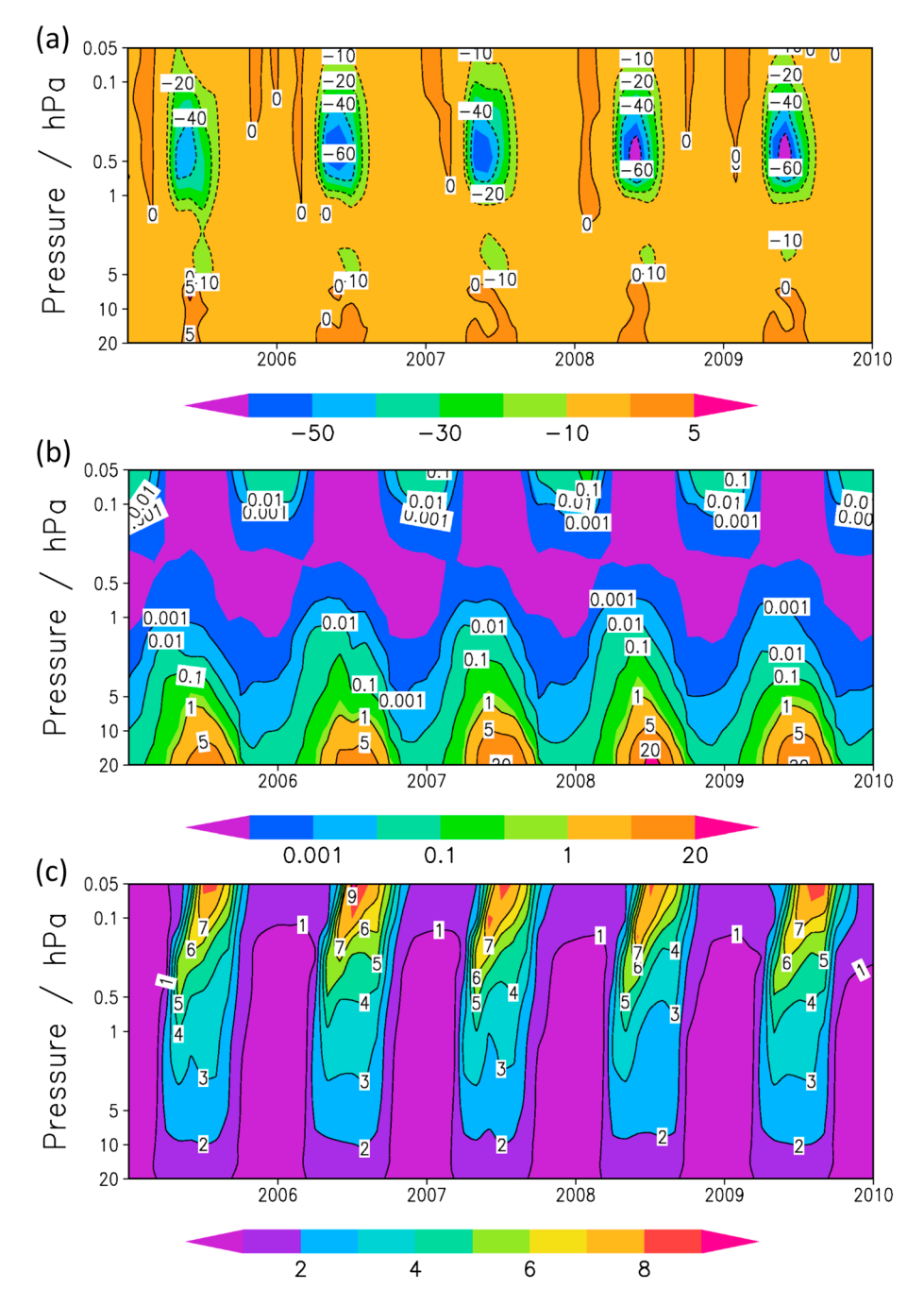


Figure 7. (a) Percentage difference in HO_2 volume mixing ratio between a WACCM-CARMA simulation with $\gamma=0.2$ and a "control" simulation with $\gamma=0$. (b) %RH in the control simulation. (c) Available surface area (μ m² cm⁻³) of MSP from the WACCM-CARMA control simulation. Data for all plots are zonally averaged at 80°S. The color bars are included to aid the reader; however, these should be treated with caution since nonlinear color scaling has been used to accentuate features in each plot.

of solar flux may be inaccurate. *Millán et al.* [2015] did not observe the overestimation at lower altitudes shown here; however, this may not be present in the more advanced off-line HO_2 retrieval used in that study. A more thorough discussion of such model discrepancies is beyond the scope of this study. Since the model broadly reproduces the observations, it is deemed a useful tool for assessing the impact of heterogeneous chemistry on the HO_2 abundance.

Figure 7a illustrates the percentage difference in HO_2 volume mixing ratio, zonally averaged at 80°S and plotted against time and altitude, between the WACCM run with HO_2 uptake and the control run. For

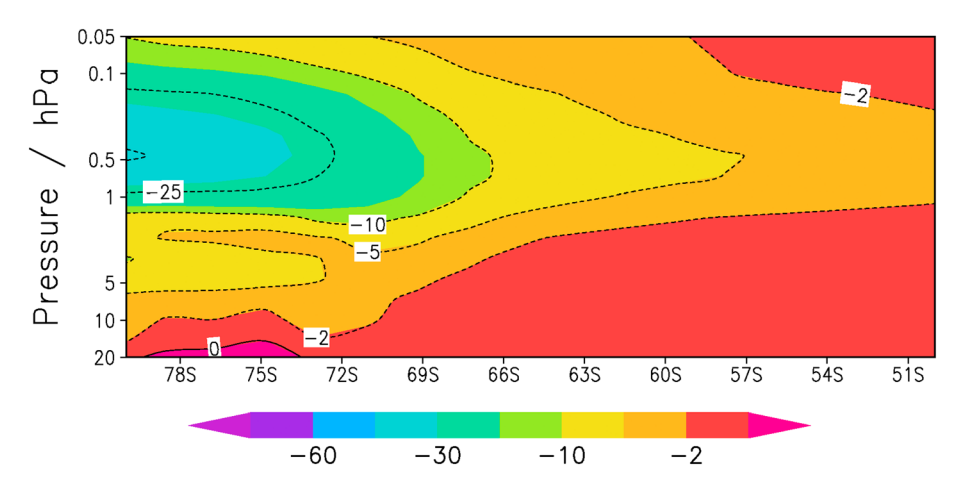


Figure 8. Percentage difference in HO_2 volume mixing ratio between the two model runs as a function of latitude for June 2009. The color bar should be interpreted with caution as nonlinear color scaling has been used to accentuate features in the plot.

comparison, the %RH and MSP surface area, both from the control run, are shown for the same region in Figures 7b and 7c, respectively. This demonstrates a clear impact on the HO_2 profile. As stated above, because of the uncertainties in both the uptake coefficient (due to temperature and RH) and surface area (due to the mass input and fractal nature of particles), the aim of this study is not to quantify such an impact but rather to demonstrate that it is potentially significant and where and when it would most likely be observed. The latitude variation of that impact is shown for June 2009 in Figure 8. The strong impact (>40% removal) near the pole falls off rapidly toward midlatitudes, with less than 10% removal at all altitudes by 65°S. This trend is qualitatively reasonable even in light of uncertainty in the uptake coefficient, since it reflects the downward transport of MSPs in the polar vortex.

Detection of the heterogeneous removal of HO_2 in the satellite observations is difficult for two reasons. First, although a 40% removal is significant, the effect is only present during the polar night (when background concentrations are relatively low) and thus difficult to identify unambiguously. Second, there is a paucity of Aura MLS measurements at very high latitudes, where the impact of MSPs is greatest. In the future, improved data sets [e.g., *Millán et al.*, 2015] may facilitate a more quantitative study. Nevertheless, the clear potential for MSPs to influence the atmospheric HO_2 profile has implications for future modeling of chemistry in the middle atmosphere.

4. Conclusions

 HO_2 uptake to MSP analogues has been studied using a combination of laboratory techniques and atmospheric modeling. A dependence on the composition of the MSP analogue was observed. This appears to be a result of mechanistic and energetic differences between the binding of HO_2 to Fe and Mg sites. Uptake coefficients, γ , of $(4.3\pm0.4)\times10^{-3}$, $(6.9\pm1.2)\times10^{-2}$, and $(7.3\pm0.4)\times10^{-2}$ were measured on forsterite, olivine, and fayalite, respectively, all at RH of ~10%.

A value for the uptake coefficient of 0.2, based on the laboratory measurements and taking into account the likely temperature and RH dependencies of γ , was applied along with a total meteoric input of 44 t day⁻¹ in WACCM-CARMA. Comparison to a control run showed that there was a significant impact on the HO₂ budget in the polar vortex, with reductions in the HO₂ volume mixing ratio of up to 40%. This impact was found to be strongly dependant on latitude, in agreement with the presence of MSPs in the polar night.

The result of the global modeling presented here should not be considered quantitatively since uncertainties in the uptake coefficient and available surface area of MSP have necessitated a rather simplistic approach. The potential for the meteoric input to be higher and the neglect of any temperature dependence of the uptake imply that this could be a lower limit to the impact of this process in the atmosphere; however, the further complications of composition and humidity dependence could offset this. Future reanalysis of Aura MLS HO₂ measurements may facilitate a more quantitative comparison by extending the latitude range covered.



Journal of Geophysical Research: Atmospheres

Acknowledgments

This work was supported by funding from the European Research Council (project 291332—CODITA). D.M. is grateful to the Natural Environment Research Council for the provision of a PhD studentship. The authors acknowledge helpful discussions with Charles Bardeen (NCAR, Boulder, CO) regarding the CARMA model. The MLS data were obtained from the NASA Goddard Earth Sciences Data and Information Services Center via ftp://acdisc.gsfc.nasa.gov/ data/s4pa/Aura_MLS_Level2. The source codes and input data for the standard WACCM/CARMA model (CESM version 1.1.1 used in this paper) are available from https://svn-ccsm-release. cgd.ucar.edu/model_versions/ cesm1_1_1 upon registration. The GEOS-5 meteorological analyses are available at https://www.earthsystemgrid.org/home.html. The WACCM data sets are archived on a University of Leeds networked server for Plane's group and available upon request to J. M.C.P. or W.F. The experimental data are available upon request to D.E.H.

References

- Bardeen, C. G., O. B. Toon, E. J. Jensen, D. R. Marsh, and V. L. Harvey (2008), Numerical simulations of the three-dimensional distribution of meteoric dust in the mesosphere and upper stratosphere, J. Geophys. Res., 113, D17202, doi:10.1029/2007JD009515.
- Broadley, S. L., B. J. Murray, R. J. Herbert, J. D. Atkinson, S. Dobbie, T. L. Malkin, E. Condliffe, and L. Neve (2012), Immersion mode heterogeneous ice nucleation by an illite rich powder representative of atmospheric mineral dust. Atmos. Chem. Phys., 12(1), 287–307.
- Brown, R. L. (1978), Tubular flow reactors with 1st-order kinetics, J. Res. Natl. Bur. Stand., 83(1), 1-8.
- Carrillo-Sánchez, J. D., J. M. C. Plane, W. Feng, D. Nesvorný, and D. Janches (2015), On the size and velocity distribution of cosmic dust particles entering the atmosphere, Geophys. Res. Lett., 42, 6518-6525, doi:10.1002/2015GL065149.
- Feng, W., D. R. Marsh, M. P. Chipperfield, D. Janches, J. Höffner, F. Yi, and J. M. C. Plane (2013), A global atmospheric model of meteoric iron, J. Geophys. Res. Atmos., 118, 9456-9474, doi:10.1002/jard.50708.
- Frankland, V. L., A. D. James, W. Feng, and J. M. C. Plane (2015), The uptake of HNO₃ on meteoric smoke analogues, J. Atmos. Sol. Terr. Phys.,
- Frisch, M. J. E. A., G. W. Trucks, H. B. Schlegel, G. E. Scuseria, M. A. Robb, J. R. Cheeseman, G. Scalmani, V. Barone, B. Mennucci, and G. A. Petersson (2009), Gaussian 09, Revision A. 01, Gaussian, Inc., Wallingford, Conn.
- George, I. J., P. S. J. Matthews, L. K. Whalley, B. Brooks, A. Goddard, M. T. Baeza-Romero, and D. E. Heard (2013), Measurements of uptake coefficients for heterogeneous loss of HO₂ onto submicron inorganic salt aerosols, Phys. Chem. Chem. Phys., 15(31), 12,829-12,845.
- Hayward, D. O., D. A. King, and F. C. Tompkins (1967), Variation of sticking probabilities with temperature and coverage, and desorption spectra for nitrogen on tungsten films, Proc. R. Soc. London A, 297(1450), 321-335.
- Hunten, D. M., R. P. Turco, and O. B. Toon (1980), Smoke and dust particles of meteoric origin in the mesosphere and stratosphere, J. Atmos. Sci., 37(6), 1342-1357.
- Lakey, P. S. J., I. J. George, L. K. Whalley, M. T. Baeza-Romero, and D. E. Heard (2015), Measurements of the HO_2 uptake coefficients onto single component organic aerosols, Environ. Sci. Technol., 49(8), 4878-4885.
- Livesey, N. J., et al. (2013), Earth Observing System (EOS) Aura Microwave Limb Sounder (MLS) Version 4.2 Level 2 Data Quality and Description Document, edited by JPL, Jet Propul. Lab., Calif. Inst. of Technol., Pasadena.
- Mao, J., et al. (2010), Chemistry of hydrogen oxide radicals (HO_x) in the Arctic troposphere in spring, Atmos. Chem. Phys., 10(13), 5823—5838. Mao, J., S. Fan, D. J. Jacob, and K. R. Travis (2013), Radical loss in the atmosphere from Cu-Fe redox coupling in aerosols, Atmos. Chem. Phys., 13(2), 509-519.
- Marsh, D. R., M. J. Mills, D. E. Kinnison, J.-F. Lamarque, N. Calvo, and L. M. Polvani (2013), Climate change from 1850 to 2005 simulated in CESM1 (WACCM), J. Clim., 26(19), 7372-7391.
- Matthews, P. S. J., M. T. Baeza-Romero, L. K. Whalley, and D. E. Heard (2014), Uptake of HO₂ radicals onto Arizona test dust particles using an aerosol flow tube, Atmos. Chem. Phys., 14(14), 7397-7408.
- Millán, L., S. Wang, N. Livesey, D. Kinnison, H. Sagawa, and Y. Kasai (2015), Stratospheric and mesospheric HO₂ observations from the Aura Microwave Limb Sounder, Atmos. Chem. Phys., 15(5), 2889–2902.
- Mozurkewich, M., P. H. McMurry, A. Gupta, and J. G. Calvert (1987). Mass accommodation coefficient for HO₂ radicals on aqueous particles. J. Geophys. Res., 92, 4163-4170, doi:10.1029/JD092iD04p04163.
- Murray, B. J., and E. J. Jensen (2010), Homogeneous nucleation of amorphous solid water particles in the upper mesosphere, J. Atmos. Sol. Terr. Phys., 72(1), 51-61.
- Murray, B. J., and J. M. C. Plane (2005), Modelling the impact of noctilucent cloud formation on atomic oxygen and other minor constituents of the summer mesosphere, Atmos. Chem. Phys., 5(4), 1027-1038.
- Pickett, H. M., et al. (2008), Validation of Aura Microwave Limb Sounder OH and HO₂ measurements, J. Geophys. Res., 113, D16S30, doi:10.1029/2007JD008775.
- Plane, J. M. C. (2012), Cosmic dust in the Earth's atmosphere, Chem. Soc. Rev., 41(19), 6507-6518.
- Plane, J. M. C., W. Feng, and E. C. M. Dawkins (2015), The mesosphere and metals: Chemistry and changes, Chem. Rev., 115(10), 4497–4541. Rapp, M., J. M. C. Plane, B. Strelnikov, G. Stober, S. Ernst, J. Hedin, M. Friedrich, and U. P. Hoppe (2012), In situ observations of meteor smoke particles (MSP) during the Geminids 2010: Constraints on MSP size, work function and composition, Ann. Geophys., 30(12), 1661.
- Saunders, R. W., and J. M. C. Plane (2006), A laboratory study of meteor smoke analogues: Composition, optical properties and growth kinetics, J. Atmos. Sol. Terr. Phys., 68(18), 2182-2202.
- Saunders, R. W., and J. M. C. Plane (2011), A photo-chemical method for the production of olivine nanoparticles as cosmic dust analogues, Icarus, 212(1), 373-382.
- Saunders, R. W., P. M. Forster, and J. M. C. Plane (2007), Potential climatic effects of meteoric smoke in the Earth's paleo-atmosphere, Geophys. Res. Lett., 34, L16801, doi:10.1029/2007GL029648.
- Saunders, R. W., S. Dhomse, W. S. Tian, M. P. Chipperfield, and J. M. C. Plane (2012), Interactions of meteoric smoke particles with sulphuric acid in the Earth's stratosphere, Atmos. Chem. Phys., 12(10), 4387-4398.
- Siskind, D. E., M. H. Stevens, C. R. Englert, and M. G. Mlynczak (2013), Comparison of a photochemical model with observations of mesospheric hydroxyl and ozone, J. Geophys. Res. Atmos., 118, 195-207, doi:10.1029/2012JD017971.
- Stone, D., and D. M. Rowley (2005), Kinetics of the gas phase HO₂ self-reaction: Effects of temperature, pressure, water and methanol vapours, Phys. Chem. Chem. Phys., 7(10), 2156-2163.
- Stone, D., L. K. Whalley, and D. E. Heard (2012), Tropospheric OH and HO₂ radicals: Field measurements and model comparisons, Chem. Soc. Rev., 41(19), 6348-6404.
- Summers, M. E., and D. E. Siskind (1999), Surface recombination of O and H₂ on meteoric dust as a source of mesospheric water vapor, Geophys. Res. Lett., 26, 1837-1840, doi:10.1029/1999GL900430.
- Thornton, J., and J. P. D. Abbatt (2005), Measurements of HO₂ uptake to aqueous aerosol: Mass accommodation coefficients and net reactive loss, J. Geophys. Res., 110, D08309, doi:10.1029/2004JD005402.
- Waters, J. W., et al. (2006), The Earth Observing System Microwave Limb Sounder (EOS MLS) on the Aura satellite, IEEE Trans. Geosci. Remote Sens., 44(5), 1075-1092.
- Whalley, L. K., et al. (2011), Quantifying the magnitude of a missing hydroxyl radical source in a tropical rainforest, Atmos. Chem. Phys., 11, 7223-7233.